Compositional editing of extracellular matrices by CRISPR/Cas9 engineering of human mesenchymal stem cell lines

Sujeethkumar Prithiviraj [1,2], Karin Linderfalk [1,2], Sonia Ferveur [1,2], Alejandro Garcia Garcia [1,2], David Hidalgo[1, 2], Ludvig Nilsén Falck [3], Agatheeswaran Subramaniam [3], Paul E Bourgine [1,2].

[1]Cell, Tissue & Organ engineering laboratory, BMC B11, 22184, Department of Clinical Sciences, Lund Stem Cell Centre, Lund University, Lund, Sweden

[2]Wallenberg Centre for Molecular Medicine, Lund University, Lund, Sweden

[3]Division of Molecular Medicine and Gene Therapy, Lund Stem Cell Centre, Lund University, 22184 Lund, Sweden

Abstract (250 words)

Tissue engineering strategies predominantly rely on the production of living substitutes, whereby implanted cells actively participate in the regenerative process. Beyond cost and delayed graft availability, the patient-specific performance of engineered tissues poses serious concerns on their clinical translation ability. A more exciting paradigm consist in exploiting cell-laid, engineered extracellular matrices (eECM), which can be used as off-the-shelf materials. Here, the regenerative capacity solely relies on the preservation of the eECM structure and embedded signals to instruct an endogenous repair. We recently described the possibility to exploit custom human stem cell lines for eECM manufacturing. In addition to the conferred standardization, the availability of such cell lines opened avenues for the design of tailored eECMs by applying dedicated genetic tools. In this study, we aim at demonstrating the possibility of exploiting CRISPR/Cas9 as a high precision system for editing the composition and function of eECMs. To this end, human mesenchymal stromal/stem cell (hMSC) lines were modified to knockout VEGF and RUNX2 and assessed for their capacity to generate osteoinductive cartilage matrices. We report the successful editing of hMSCs, subsequently leading to targeted VEGF and RUNX2-knockout cartilage eECMs. Despite the absence of VEGF, eECMs retained full capacity to instruct ectopic endochondral ossification. Conversely, RUNX2-edited eECMs exhibited impaired hypertrophy which resulted in delayed bone formation in vivo. In summary, our approach can be harnessed to identify the necessary eECM factors driving endogenous repair. Our work paves the road towards the compositional eECMs editing and their exploitation in broad regenerative contexts.

31 **Introduction**

32 Extracellular matrices (ECMs) are complex networks of proteins providing tissue structural and mechanical
33 support, but also acting as growth factor storing and presenting entities[1]. As such, ECMs are receiving
34 increasing attention in tissue engineering as templates capable of guiding homeostasis, remodeling and
35 regenerative processes[2,3,4].
36 ECMs can be derived from native tissue or organs (native ECMs, nECMs) by applying a decellularization
37 step which effectively removes the cellular fraction. The resulting nECMs are commonly used as
38 biomaterials in regenerative medicine[5,6], offering a natural biocompatible structure. However, they suffer
39 from substantial batch-to-batch variation with their properties being largely affected by the tissue source
40 and the decellularization process[5,6]. Importantly, while displaying a high level of biological complexity and
41 fidelity, the composition of nECMs cannot be tailored to specific needs.
42 A valuable option emerged from recent advances in bioengineering which led to the development of
43 synthetic ECMs (sECMs). These tunable materials are predominantly composed of biopolymers such as
44 poly(lactic acid) (PLA), poly(glycolic acid) (PGA), poly(lactic co-glycolic acid) (PLGA) and Poly (ethylene
45 glycol) (PEG), which can be functionalized with bioactive substances such as peptides, growth factors or
46 enzymes[3,7,8,]. The possible modulation of sECM's composition and chemistry offers precise control over
47 their mechanical properties, degradability, and temporal release of instructive molecules towards
48 improved tissue repair. Despite holding great promises, yet their structure and function remain simplified
49 compared to their native counterpart [9,10].
50 With the aim of combining high biological fidelity and design flexibility, engineered ECMs (eECMs) have
51 become a credible alternative. Those consist in the exploitation of stem/progenitor populations capable
52 of depositing ECMs under specific in vitro culture conditions[11,12,13,14], which can be subsequently isolated
53 from the cellular fraction and exploited as a cell-laid product. Early studies were conducted using eECM
54 derived from primary cells, exhibiting variable performance associated with the inter-donor variability[15,16].
55 Most recently, we demonstrated the possibility to standardize the production of eECMs through the
56 engineering of dedicated human mesenchymal stromal/stem cell (hMSC) lines[17]. Precisely, the
57 Mesenchymal Sword of Damocles – BMP2 (MSOD-B) line offered the generation of eECMs in the form of
58 human cartilage templates[18]. Those cartilage templates can be further devitalized, lyophilized and stored
59 as an *off-the-shelf* tissue, retaining remarkable bone formation capacity by instructing endochondral
60 ossification[18,19].
61 The exploitation of cell lines as an unlimited cell source for eECM generation offers unprecedented
62 standardization in graft production and performance. Meanwhile, it also consists of a robust cellular

63 platform facilitating their further genetic engineering, to achieve the production of eECMs tailored in
64 composition and function. Towards this objective, CRISPR/Cas9 appears as a versatile and efficient gene-
65 editing tool. While this technology has been extensively used for genetic screening or disease
66 modeling[20,21,22], the possibility to edit hMSCs and study the compositional impact on deposited eECMs has
67 not been investigated so far.
68 In this study, we aim at demonstrating that CRISPR/Cas9 can be applied as an editing tool for the
69 engineering of custom eECMs. As proof-of-principle, our strategy relies on the CRISPR/Cas9-guided editing
70 of the MSOD-B line for knocking out Vascular endothelial growth factor (VEGF) and Runt related
71 transcription factor 2 (RUNX2), respectively a key pro-angiogenic protein and transcription factor critically
72 involved in the endochondral ossification pathway. The resulting hMSC lines will be evaluated for their
73 capacity to generate hypertrophic cartilage in vitro and instruct in vivo bone formation as a cell-free and
74 lyophilized template. If successful, our study is expected to validate the use of CRISPR/Cas9 for eECMs
75 edited in composition, while providing a novel platform towards decoding the necessary molecular signals
76 driving effective tissue repair.
77

78 **Results**

79 **CRISPR/Cas9 editing of hMSC lines lead to efficient VEGF knockout in cartilage tissues**

80 VEGF is a known master regulator of angiogenesis[23] and a key mediator of endochondral ossification.
81 When reaching hypertrophy, chondrocytes highly express VEGF, prompting vasculature invasion and
82 subsequent osteoprogenitor recruitment. This was proven to be essential for cartilage template
83 remodeling into bone and bone marrow[24]. Here, we thus first aimed at engineering a hMSC line
84 CRISPR/Cas9-edited for VEGF knockout and evaluate the corresponding impact on cartilage and
85 endochondral bone formation (Figure 1A). To this end, specific guide RNAs (gRNAs) targeting different
86 regions of the VEGF gene but conserved across all isoforms of VEGF were designed based on a previously
87 established protocol[25]. Three gRNAs targeting exon 1 (VEGF_1.1, VEGF_1,2, VEGF1.3), one targeting exon
88 2 (VEGF_2.1), and one targeting exon 8 (VEGF_8.1) were designed (Figure 1B, Supplementary Figure 1A).
89 These gRNAs were cloned into the pU6-(BbsI)_CBh-Cas9-T2A-mCherry vector encoding the Streptococcus
90 pyogenes Cas9 (SpCas9) machinery. Following transfection in MSOD-B cells, single cell clones were sorted
91 based on the transient mCherry expression and expanded for characterization (Figure 1A). Out of 163
92 single clones, 14 could be successfully expanded (8.5 %). From these clones, five were retrieved from the
93 gRNA 1.1, six from gRNA 1.3 and three from gRNA 8.1. In order to assess a successful editing and directly

94 correlate it to a knockout of VEGF, an ELISA assay was performed to measure the concentration of VEGF
95 in the supernatant of expanded MSOD-B clones (Figure 1C). In non-edited cells (MSOD-B, control), 5000
96 pg/mL were secreted and detected by ELISA. From the successfully expanded clones, most of them
97 showed reduced but non-abolished secretion of VEGF. However, two clones exhibited undetectable levels
98 of VEGF, both resulting from the gRNA targeting the Exon1 of the VEGF gene. These clones were defined
99 as MSOD-BΔV1 and MSOD-BΔV2 and further characterized for their capacity to form cartilage.

100 To this end, clones were expanded and seeded on collagen scaffold and induced for three weeks towards
101 chondrogenic differentiation. As anticipated with the MSOD-B tissues, histological assessment revealed
102 the formation of a collagenous matrix (Masson's Trichrome) with cartilage features (Safranin-O, Figure 1D
103 and Supplementary Figure 1B). Similarly, a successful chondrogenic differentiation and deposition of
104 glycosaminoglycans could be observed in the MSOD-BΔV1 (Figure 1D) and MSOD-B ΔV2 (Supplementary
105 Figure 1B) constructs. A quantitative assessment (blyscan assay) confirmed the comparable content in
106 glycosaminoglycans in MSOD-B and VEGF-edited clones (Figure 1E, Supplementary Figure 1C).
107 Importantly, VEGF quantification in corresponding pellets validated the successful knockout of the
108 protein, barely detectable in the MSOD-BΔV1 and ΔV2 tissues (47.64 pg/pellet in edited clones versus
109 552.7 pg/pellet in MSOD-B, Figure 1F and Supplementary Figure 1D).

110 Taken together, this data indicates the successful generation of MSOD-B lines knocked-out in VEGF. The
111 MSOD-BΔV1 and MSOD-BΔV2 clones exhibited frank cartilage formation capacity with minimal level of
112 VEGF. This validates the use of CRISPR/Cas9 as a precision tool to edit the composition of cartilage tissue.

113

114 **VEGF knockout cartilage tissues retain bone remodeling capacity despite reduced early-stage**
115 **vascularization**

116 To verify the impact of the VEGF knockout on the graft capacity to undergo endochondral ossification,
117 cartilage grafts were implanted subcutaneously in an immunodeficient mouse model. Importantly, prior
118 to implantation, tissues were lyophilized using a pre-established protocol[18]. This allowed us to assess the
119 performance of the generated tissue itself, in line with the idea of developing off-the-shelf substitutes.
120 Samples were extracted after two and six weeks as early and late development timepoints. Since the two
121 clones exhibited similar in vitro tissue formation capacity, only the MSOD-BΔV1 was selected for in vivo
122 performance assessment. After two weeks in vivo, we first evaluated the angiogenic potential of tissues
123 by quantitative confocal microscopy imaging of 100 µm thick sections stained for CD31, a well-defined

124 marker for angiogenesis. This allowed us to evidence a dense vascular network in MSOD-B constructs,
125 covering the entirety of the grafts (Figure 2A). Instead, MSOD-BΔV1 displayed a more limited
126 vascularization, pre-dominant at tissue periphery (Figure 2A). Quantification confirmed these
127 observations with MSOD-B exhibiting a significantly higher volume of vessels per total section volume
128 (0.191 % versus 0.132 % for MSOD-B and MSOD-BΔV1 respectively, Figure 2B).

129 Using microtomography, we further assessed the amount of mineralized tissue formed in a temporal
130 fashion. At two weeks, the formation of a cortical ring of mineralized tissues could already be observed in
131 both MSOD-B and MSOD-BΔV1 tissues (Figure 2C). Quantifications revealed a similar bone/mineralized
132 volume normalized to the total volume of the graft (BV/TV, Figure 2D) with 0.17 % and 0.16 % in MSOD-
133 B and MSOD-BΔV1 samples respectively. At the six-week timepoint, trabecular structures could be
134 observed in reconstructed 3D scans from both groups (Figure 2C). Remarkably, histological analysis
135 confirmed the similar development of the tissues with frank bone formation (Masson´s trichrome) already
136 at two weeks post-implantation and minimal remnants of cartilage (Safranin O) (Figure 2E). At six weeks
137 both samples remodeled into fully mature bone organs, characterized by presence of cortical and
138 trabecular structures as well as a bone marrow tissue filling the cavity (Figure 2E).

139 These results indicate that the absence of VEGF in cartilage tissue can delay the early vascularization of
140 MSOD-BΔV samples. However, this did not prevent nor impact the remodeling of the lyophilized grafts
141 into bone and bone marrow tissues indicating that VEGF is non-essential in order to efficiently instruct
142 endochondral ossification.

143

144 **RUNX2 knockout does not prevent chondrogenic differentiation but impairs hypertrophy**

145 We next investigated whether the composition and thus function of a graft could be modified by editing
146 transcriptional factors involved in mesenchymal cell differentiation. Using CRISPR/Cas9, we thus targeted
147 the RUNX2, a known master regulator particularly important for chondrocyte differentiation and
148 hypertrophy[26,27]. We designed gRNAs targeting the coding regions involved in cell signaling integration,
149 activation, and inhibition domain which are conserved in both isoforms of RUNX2 (Figure 3A,
150 Supplementary Figure 3A).

151 One gRNA was designed for targeting exon 2 (RUNX2_2.1), one targeting exon 5 (RUNX2_5.1), two
152 targeting exon 6 (RUNX2_6.1 and RUNX2_6.2) and one targeting exon 8 (RUNX2_8.1). Similar to the VEGF
153 set-up, gRNAs were transfected in MSOD-B cells together with a pU6-(BbsI)_CBh-Cas9-T2A-mCherry

154 plasmid to ensure transfection efficiency and single cell sorting of positive clones. Out of 385 single clones,
155 62 could be successfully expanded, corresponding to a 16.1% efficiency. From these clones, five were
156 derived from the RUNX2_5.1 gRNA, 18 from RUNX2_6.1, 15 from RUNX26.2 and 24 from RUNX2_8.1.

157 To identify successfully edited clones, we first screened for those exhibiting a decrease in their RUNX2
158 protein expression using intra cellular flow cytometry. Among the 62 clones, 17 displayed a reduced
159 RUNX2 pattern as compared to the MSOD-B control (Figure 3B and Supplementary Figure 3B) and were
160 further sent for sequencing analysis. This led to the identification of two successfully edited clones,
161 demonstrating a point mutation in the exon 6 of RUNX2 gene (Supplementary Figure 3C). To confirm the
162 knockout impact on the transcription factor structure, a Western Blot analysis was conducted on cellular
163 extracts of in vitro cultured cells. MSOD-B cells exhibited intact RUNX2 proteins of 52 - 62 kDa[28,29](Figure
164 3C). Instead, the RUNX2-edited cells displayed truncated versions of 32 - 42 kDa, consistent with the
165 expected mRNA shortening.

166 These two clones were defined as MSOD-BΔR1 and MSOD-BΔR2 and further assessed for their ability to
167 form cartilage in vitro. Following 3D chondrogenic differentiation, samples were processed for histological
168 analysis. The presence of cartilage structures embedded in a rich collagenous matrix could be observed in
169 all MSOD-B, MSOD-BΔR2 (Figure 3D) and MSOD-BΔR1 tissues (Supplementary Figure 3D). Quantification
170 of glycosaminoglycans revealed a similar content in all the groups (Figure 3E, Supplementary Figure 3E).
171 Using immunostaining combined with quantitative confocal microscopy, the possible impact of RUNX2-
172 editing on tissue hypertrophy was further investigated. First, Collagen Type II (COL2) staining confirmed
173 the similar distribution of cartilage matrix across MSOD-B, MSOD-BΔR1 and MSOD-BΔR2 samples (Figure
174 3F and Supplementary Figure 3F). However, we observed a clear distinction in the Collagen Type X (COLX)
175 expression pattern, a specific marker of hypertrophy which was hardly detectable in MSOD-BΔR tissues
176 (Figure 3F and Supplementary Figure 3F). Subsequent quantification confirmed a significant reduction of
177 COLX volume in MSOD-BΔR1 (0.46 %) and MSOD-BΔR2 (0.32 %) compared to MSOD-B (0.81 %) (Figure 3G,
178 Figure 3H, Figure 3I).

179 In summary, we here report the successful RUNX2 knockout in MSOD-B lines using CRISPR/Cas9. RUNX2
180 did not impair chondrogenesis but prevented the tissue hypertrophy, evidenced by residual COLX content
181 in engineered cartilages.

182

183

184 **RUNX2 knockout in cartilage tissues disrupts effective bone formation**

185 To assess the corresponding impact of RUNX2-edited cartilages on bone formation, MSOD-B tissues (as
186 control) and MSOD-BΔR1 were lyophilized and implanted subcutaneously in immunodeficient mice for
187 two to six weeks. From microtomography image reconstructions, we observed an evident reduction of
188 mineralization in MSOD-BΔR1 compared to MSOD-B (Figure 4A) already after two weeks. This qualitative
189 and visual difference in mineralization persisted after six weeks in vivo (Figure 4A). Subsequent
190 quantifications confirmed these observations with a clear reduction in BV/TV as early as week 2 (16.46 %
191 in MSOD-B and 7.01 % in MSOD-BΔR1) and persisting at week 6 (20.03% in MSOD-B and 4.25 % in MSOD-
192 BΔR1) (Figure 4B). Histological analysis revealed an early bone formation at two weeks in both samples,
193 but to a lower extent in the MSOD-BΔR1 group (Figure 4C). As anticipated, MSOD-B tissues underwent full
194 remodeling after six weeks in vivo. In sharp contrast, the MSOD-BΔR1 only displayed a partial maturation
195 with limited presence of bone and bone marrow.

196 Altogether, this indicates an incomplete remodeling of RUNX2 edited samples with significantly delayed
197 cortical and trabecular structure formation. This correlates with the impaired hypertrophic phenotype in
198 the corresponding in vitro samples.

199

200 **Discussion**

201 We here report the possibility to edit the composition and function of eECM by CRISPR/Cas9 engineering
202 of human mesenchymal lines. VEGF knockout led to successful in vitro formation of cartilage with targeted
203 protein depletion. Upon implantation, this impacted the graft vascularization onset but not the
204 endogenous instruction of the endochondral program. In turn, RUNX2 knockout prevented cartilage
205 hypertrophy in vitro, significantly delaying bone and bone marrow formation in vivo.
206 A clear interdependency of angiogenesis and osteogenesis occurs upon bone formation[30,31]. For this
207 reason, VEGF-enrichment has been naturally proposed as a strategy to accelerate or increase bone graft
208 vascularization[32,33]. Our study demonstrates that VEGF knocked-out cartilage templates retained full
209 osteoinductive potential in a challenging ectopic environment. Those results are in sharp contrast with
210 intramembranous strategies[34,35], including our previous work[17], whereby grafts remain insufficient in
211 promoting complete bone remodeling even upon VEGF-enrichment. This suggests that the first stage of
212 host progenitor recruitment by our eECM is not VEGF dependent, although subsequent tissue
213 vascularization and remodeling may be orchestrated in a second step by endogenous cell secretion. Other

214 pro-angiogenic proteins embedded in the matrix may also have compensated for the lack of VEGF, such
215 as BMP-2[18] known to stimulate endothelial cell proliferation, migration and differentiation[36,37].
216 Conversely, RUNX2 deletion was shown to fully prevent cartilage hypertrophy, in line with published
217 mouse models also reporting a lack of endochondral ossification and lethality at birth upon RUNX2
218 knockout[38,27]. Here, MSOD-BΔR cartilage templates still exhibited frank bone formation capacity, but with
219 cortical and trabecular structures largely reduced as compared to controls. Future work may clarify if this
220 strictly results from the absence of COLX, or if an additional specific cartilage matrix component (e.g.
221 matrix metalloproteinases) impaired the instruction of endochondral ossification.
222 CRISPR/Cas9 editing of human mesenchymal cells has previously been explored for gene and cell therapy
223 applications[20,21] , for tailoring the immunomodulatory and/or differentiation capacity of engineered cells.
224 However, no studies have described the exploitation of editing strategies for the generation of eECMs,
225 whereby modified cells are absent from the final grafting product. Our work illustrate that this can be
226 achieved by direct targeting of secreted factors typically embedded upon ECM deposition, as
227 demonstrated with VEGF. Alternatively, we also propose the knockout of key transcription factors as a
228 strategy for custom eECM generation by impacting their tissue developmental/maturation stages.
229 A clear implication of our work lies in the possibility to decipher the necessary factors capable of
230 instructing de novo tissue formation. Those findings will be of high relevance for the design of eECMs
231 tailored in composition. Beyond bone repair, our study also bears high relevance in other regenerative
232 contexts. In fact, one could envision further preventing the in vivo remodeling of engineered cartilage
233 templates and obtain stable cartilage graft for joint repair[39,40]. This remains an open challenge in the
234 skeletal field, with bone marrow MSCs (BM-MSCs) cartilage systematically reaching hypertrophy and
235 subsequent ossification[41,42,43]. An exciting opportunity also lies in harnessing CRISPR/Cas9 for editing
236 eECMs and tuned their immunogenicity. Key inflammatory components could be turned down, leading to
237 improved efficacy of repair in line with the immuno-engineering principles[44,45] .
238 Importantly, our study describes the exploitation of eECMs in a lyophilized form, thus conferring an off-
239 the-shelf storage solution. Together with the standardization of production conferred by stable cell
240 sources, our concept offers exciting translational opportunities. In fact, instrumental to this work is the
241 use of dedicated hMSC lines. The genetic modification of primary cells is laborious, and their limited
242 lifespan ex vivo challenges their selection, characterization and exploitation for tissue engineering
243 applications[46,47]. Here, the MSOD-B was harnessed as an unlimited cell source with robust differentiation
244 potential. Nonetheless, the editing of eECMs remains tedious in part due to the limited CRISPR/Cas9
245 efficiency and potential off-target effects, calling for a systematic clonal selection. In addition, while large

246 CRISPR/Cas9 screening can be performed in other stem cell systems[48,49], the critical cell mass required for
247 effective cartilage formation affects parallelization and leads to limited throughput. Nonetheless, after
248 the identification and characterization process, the resulting cell lines can be banked and used for
249 unlimited tissue manufacturing.
250 The MSOD-B line remains the only human cell source capable of priming endochondral ossification by
251 engineering living or cell-free grafts. This was demonstrated to be driven by the combined low dose of
252 BMP-2 embedded in the tissue (~40 ng/tissue) together with glycosaminoglycans and other thousands of
253 identified ECM proteins[18]. The BMP-2 amount is thus far below the typical amount used in sECMs
254 approaches for effective osteoinduction, falling in the microgram to milligram range[18]. This is one key
255 advantage of eECM graft, exhibiting a biological complexity that so far has not been matched by sECMs.
256 Ideally, the two approaches are complementary as the editing of eECMs could inform on the necessary
257 but sufficient factors driving effective regeneration. Those would in turn be embedded in a sECMs strategy
258 and offer a fast and possibly cost-effective solution.
259 To conclude, the present work offers a platform for decoding factors involved in tissue regeneration and
260 generate tailored eECM. Here, illustrated in the context of skeletal repair, our study may offer similar
261 opportunities in other regenerative situations.

262 **Acknowledgements**
263 We express our gratitude to the following institutions and individuals for their invaluable support and
264 contributions to this study: Lund University, Medical Faculty, FACS Facility (Anna Hammarberg), Cell and
265 Gene Therapy core facility (Pia Johansson) and Imaging Facility at Lund Stem Cell Centre, as well as the
266 Lund University Bioimaging Centre, for providing access to the X-ray CT system. The funding for this
267 research was made possible by a Knut and Alice Wallenberg grant, the Medical Faculty at Lund University,
268 the Swedish Research Council, the European Research Council (Starting grant hOssicle #948588 to P.E.B),
269 and Region Skåne. Figures were generated using BioRender.com. Special thanks to Ani Grigoryan and
270 Dimitra Zacharaki for their expertise and valuable insights regarding FACS experiments, and to Steven
271 Dupard for his advice and guidance on the design of gRNAs and molecular techniques. Christian Hansen
272 deserves our appreciation for providing the mcherry plasmid and offering valuable guidance and
273 knowledge related to CRISPR-Cas9.

274

275 **Materials and Methods:**
276 **Cell expansion**

277 MSOD-B cells and their modified progeny were cultured in a humidified incubator at 37 °C and 5% CO_2
278 using complete medium consisting of α-minimum essential medium (αMEM) supplemented with 10%
279 fetal bovine serum, 1% HEPES, 1% sodium pyruvate, 1% penicillin-streptomycin-glutamine solution, and 5
280 ng/ml of fibroblast growth factor-2 (FGF-2) (all from Gibco). Cells were seeded at a density of 3200
281 cells/cm^2 until they reached 90% confluency. The medium was replaced twice a week.

282 **Chondrogenic differentiation**

283 MSOD-B cells and their modified progeny were harvested from culture flasks by adding Trypsin-EDTA
284 (0.25%) (Gibco) and subsequently seeded on cylindrical Collagen Type I scaffold (Avitene™ Ultrafoam™
285 Collagen Sponge, Davol) of 6 mm in diameter and 3 mm in thickness at a density of 2 x 10^6 cells per scaffold
286 in 12 well plates coated with 1 % agarose (Sigma). Tissue constructs were cultured for three weeks in
287 chondrogenic medium (DMEM supplemented with 1% penicillin-streptomycin-glutamine, 1% HEPES (1M),
288 1% sodium pyruvate (100 mM), 1% ITS (100x) (Insulin, Transferrin, Selenium) (all from Gibco), 0,47 mg/ml
289 linoleic acid (Sigma), 0.12% bovine serum albumin (25 mg/mL) (BSA) (Sigma), 0.1 mM ascorbic acid
290 (Sigma), 10^{-7} M dexamethasone (Sigma) and 10 ng/ml TGF-β3 (Novartis)). Media were replaced twice a
291 week.

292 **Lyophilization**

293 After three weeks of chondrogenic differentiation, the tissue constructs were rinsed twice with PBS 7.2
294 (without calcium/magnesium Gibco), snap frozen in liquid nitrogen for five minutes and then lyophilized
295 using a freeze dryer (-80 °C and 0.05 mbar) overnight. Thereafter, the lyophilized tissue constructs were
296 stored at 4 °C.

297 **Transfection of MSOD-B cells with gRNAs**

298 MSOD-B cells were seeded at a density of 400,000 cells per well in 12 well plates to reach a minimum of
299 80% confluency the following day. The medium was replaced before transfection. The transfection was
300 performed with a / ratio of 2 µL lipofectamine to 1 µg DNA. A DNA mix was prepared for each of the five
301 gRNAs and the two plasmid controls. DNA mixtures were composed of 1 µg of plasmid, 2 µL of P3000
302 reagent and 50 µL of OptiMEM (Thermo-Fischer). A lipofectamine cocktail was prepared for all DNA
303 mixtures consisting of 24 µL of lipofectamine 3000 in 400 µL of OptiMEM. Lipofectamine and the DNA
304 mixtures were added at a 1:1 ratio. After 48h, cells were analyzed and mCherry positive clones were FACS
305 sorted as single cells in 96-well plates using ARIAIII (BD Biosciences). Successfully expanded clones were
306 then further characterized.

307 **ELISA**

308 VEGF protein content was measured in supernatant collected from cells seeded at 100´000 in T175 flask

309 and cultured for 3 days. Content from engineered cartilage tissues was assessed following digestion in
310 RIPA buffer. The Quantikine ELISA kit for Human VEGF-A Immunoassay from the R&D System was used
311 according to the manufacturer instructions to determine protein concentration.

312 **Intracellular flow cytometry**

313 MSOD-B and MSOD-B ΔRUNX2 cells were trypsinized, fixed and permeabilized using the
314 Fixation/Permeabilization Kit (BD Biosciences). Following a blocking step in 10% normal donkey serum
315 (Sigma), cells were stained with a primary antibody against RUNX2 (Rabbit anti-human, Thermo-Fischer
316 PA5-82787) for one hour at room temperature. After primary antibody incubation, cells were washed and
317 stained with an Allophycocyanin (APC) labeled secondary antibody (Donkey anti-rabbit IgG DyLight™ 649,
318 Biolegend 406406) for 30-45 minutes at room temperature in 2% normal donkey serum. The Control
319 samples consisted of unstained cells (negative control) and cells incubated only with the secondary
320 antibody (secondary Ab control). Data were recorded on a BD LSRFortessa™ Cell Analyzer (BD
321 Biosciences). FCS files were analyzed using the FlowJo™ software (FlowJo LLC, 10.5.3, BD Biosciences).

322 **Western blotting**

323 MSOD-B and MSOD-B ΔRUNX2 cells were trypsinized and washed with ice cold PBS twice and lysed on ice
324 for 10 min in RIPA buffer (#10017003, Thermo Fisher Scientific) supplemented with 1× proteinase and
325 phosphatase inhibitor cocktail (#78440, Thermo Fisher Scientific). The lysates were centrifuged at 16,
326 000*g* for 15 min +4 °C, and the supernatants were collected. Sample buffer (Laemmli buffer (#161-0737,
327 BioRad) supplemented with 5% 2-mercaptoethanol, 1× proteinase and phosphatase inhibitor cocktail
328 (#78440, Thermo Fisher Scientific) was added to the supernatant at 1:1 ratio. Samples were boiled at 95
329 °C for 5 minutes and stored at −80 °C or kept on ice until gel loading. Proteins were separated using Bolt
330 gels according to manufacturer's protocol (#NW04122, #B0002, Thermo Fisher Scientific). iBlot2 system
331 was used to transfer the proteins on polyvinylidene fluoride membrane (PVDF) membrane according to
332 manufacturer's protocol (#IB24001, Thermo Fisher Scientific). PVDF membrane was washed once in 1×
333 PBST buffer (#28352, Thermo Fisher Scientific) and blocked in 2% blocking solution (#10156414, Thermo
334 Fisher Scientific) for 1 h at room temperature. Membranes were incubated overnight at +4 °C with primary
335 antibodies at recommended concentrations in 1% blocking solution. Membranes were washed three
336 times (5 min for each wash) with 1× PBST buffer, and secondary HRP-conjugated antibodies in 1% blocking
337 solution were added to the membranes at 1:5000 concentration for 1 h incubation at room temperature.
338 Membranes were washed three times with 1× PBST and proteins were detected by chemiluminescence
339 according to manufacturer's protocol (#RPN2232, Thermo Fisher Scientific). The following antibodies
340 were used. primary antibodies: RunX2 (D1L7F - 12556) from Cell Signaling Technology and Actin (612656)

341 is from Becton Dickinson. The secondary antibodies were anti-Mouse (GENA931) from Sigma-Aldrich, anti-
342 Rabbit (NA9340V) from Thermo Fisher Scientific.

343 **Biochemical analysis (GAG analysis)**

344 Lyophilized tissue constructs were digested by overnight incubation in 0.5 ml of Proteinase K solution
345 (Proteinase K 1 mg/mL, Sigma; pepstatin A 10 ug/ml, Sigma; 1 mM EDTA, Sigma; Iodoacetamide 100 mM;
346 Tris 5 0mM) at pH 7.6 and 56 °C. The GAG content of digested samples was analyzed using
347 Glycosaminoglycan Assay Blyscan kit (Biocolor) following the manufacturer instruction.

348 **Mice**

349 FoxN1 KO BALB/C (nude mice) 6–8-weeks old, were obtained from Charles River Laboratories. All mouse
350 experiments and animal care were performed in accordance with the Lund University Animal Ethical
351 Committee guidelines (ethical permit #M15485–18). Mice were housed at a 12-hour light cycle in
352 individually ventilated cages at a positive air pressure and constant temperature. Mice were fed with
353 autoclaved diet and water ad libitum. During the implantation procedure, anaesthesia was performed
354 with 2-3 % Isoflurane (Attane). The mice were kept on a heating pad during the procedure to avoid the
355 heat loss.

356 **Micro-CT scanning**

357 In vivo samples were explanted and fixed overnight with 4% formaldehyde before ex vivo micro-CT
358 analysis using a U-CT system (MILABS, Netherland) equipped with a tungsten x-ray source at 50 kV and
359 0.21 mA. Volumes were reconstituted at 10 µm isotropic voxel size and were saved as. nii files. For total
360 volume (TV) analysis, each sample was assessed with Blender (v2.82a, Netherland). First, the .nii file was
361 opened in Fiji software, applying default parameters, and accessing the 3D Viewer Plugin. The threshold
362 level was adjusted to identify the Ossicle, and the resulting surface was saved as .obj and .mtl files in
363 Blender. Subsequently, the .obj file was imported into Blender, followed by remeshing and centering the
364 sample within the cage. The "shrinkwrap" volume dialogue box was utilized to position the sample within
365 the network. The volume was then calculated and obtained in cm^3. For bone volume (BV) analysis, the
366 highly mineralized tissue volume was quantified using Seg3D (v2.2.1, NIH, NCRR, Science Computing and
367 Imaging Institute (SCI)). The .nii file was converted to BMP files in Fiji. Seg3D was employed to import the
368 BMP files and create a threshold layer highlighting the bone. The sample was then converted into a 3D
369 representation, and the BV was calculated based on pixel units. To obtain the volume in mm^3, the value
370 was divided by 1,000,000, taking into account the appropriate voxel size.

371 **Sample preparation for histological analysis**

372 In vitro samples were directly fixed prior to sectioning. In vivo samples were fixed and subsequently
373 decalcified with a 10% EDTA solution, pH = 8, at 4 °C for two weeks prior to tissue embedding.
374 Paraffin embedding was performed on samples fixed in 4% formalin (Solveca AB). Tissues were
375 dehydrated by immersion in consecutive solutions of 35%, 70%, 95%, and 99.5% graded ethanol solution
376 (Solveco AB). Immersion in a 99.5% ethanol/xylene solution (1:1, Fisher Scientific) was then performed
377 for ten minutes followed by two rinsing in xylene (Fisher Scientific) for 20 minutes. Subsequently,
378 tissues were embedded in paraffin at 56 °C overnight, before sectioning with a microtome (Microm HM
379 355 Rotary Microtome) in 5 - 10 µm sections. The sections were then dried overnight at 37 °C before
380 staining. Prior to staining, sections were deparaffinized by two washes in xylene for 7 minutes and once
381 in 99.5% ethanol/xylene solution (1:1) for 3 minutes. Afterwards, sections were hydrated twice in
382 consecutive solutions of 99.5%, 95%, 70%, and 35% ethanol, for 7 minutes each.

383 Agarose embedding was performed on samples fixed overnight with 4% paraformaldehyde (Thermo
384 Scientific), using 4% low-melting agarose (Sigma). Sections of 100 µm thickness were obtained using a
385 7000smz vibratome (Campden) with stainless steel or ceramic blades.

386 **Safranin O Staining**

387 Paraffin-embedded sections were stained using Mayer's hematoxylin solution (Sigma-Aldrich) for 10
388 minutes. Samples were then placed under running distilled water to remove superfluous staining from
389 the sections. Subsequently, sections were stained with 0.01% fast green solution (Fisher Scientific) for five
390 minutes, and rinsed with 1% acetic acid solution (0.5 ml acetic acid in 49.5 ml distilled water) for
391 15 seconds. After that, the slides were stained with 0.1% safranin O (Fisher Scientific) solution for 5
392 minutes. Dehydration and clearing were performed by immersion in 95%, 99.5% ethanol, 99.5%
393 ethanol/xylene solution (1:1) and xylene twice successively for 2 minutes. Finally, the stained slides were
394 mounted with glass slides using PERTEX mounting medium (PERTEX, HistoLab).

395 **Masson's trichrome staining**

396 Masson's trichrome staining was performed using the trichrome staining kit (Sigma-Aldrich Sweden AB)
397 according to the manufacturer's guidelines. Briefly, tissue sections were deparaffinized and immersed in
398 cold running deionized water for 3 minutes. Then the sections were kept in Bouin's solution at room
399 temperature overnight or at 56 °C for 15 minutes. The slides were washed by running tap water and
400 stained using working Weigert's iron hematoxylin solution (Sigma) for five minutes for nuclei detection
401 (in black). After washing the slides, the cytoplasm was stained in red with Biebrich Scarlet-Acid fuchsin for
402 five minutes followed by clearing the slides by immersion in working phosphotungstic/ phosphomolybdic
403 acid solution (25 ml P. tungstic + 25 ml P. molybdic+ 50 ml distilled water) for five minutes. Collagen

404 stained blue by immersion in aniline blue solution for five minutes followed by clearing in 1% acetic acid
405 solution diluted in distilled water (glacial, Fisher Scientific) for two minutes and washing with running
406 deionized water. Finally, the sections were dehydrated in graded ethanol solutions (95% once, 100%
407 twice) for two minutes each before washing with xylene twice for two minutes and mounted with PERTEX
408 mounting medium.

409 **Immunofluorescence**

410 Agarose-embedded sections were treated with 0.5% Triton X-100 (Sigma) in PBS supplemented with 20%
411 donkey serum (Jackson ImmunoResearch) for one hour at room temperature (RT) for blocking and
412 permeabilization. After blocking/permeabilization, sections were stained with primary antibodies (mouse
413 anti-Collagen II (Invitrogen, MA137493), rabbit anti-Collagen Type X (ColX) (abbexa, abx101469),) at 4 °C
414 overnight. Sections were washed three times using cold PBS with 0.1% Triton X-100, 20 minutes each,
415 followed by staining with secondary antibodies (CF568 donkey anti-rabbit (Biotium, 20098), CF633 donkey
416 anti-mouse (Sigma-Aldrich, SAB4600131 in 2% donkey serum for three hours at room temperature.
417 Sections were washed three times using cold PBS with 0.1% Triton X-100, 20 minutes each once more. For
418 vasculature assessment, paraffin-embedded sections were stained following a previously established
419 protocol[50] (primary antibody: Goat anti mouse/rat CD31 (R&D system, YZU0119121), secondary antibody:
420), CF567 anti-goat (Invitrogen, A11057)).

421 All sections were mounted using the Vectashield antifade mounting medium containing DAPI (Vector
422 Laboratories, H1200). A LSM780 confocal microscope (Zeiss) with a 10x/20x objective was used to capture
423 images and image series of whole tissue sections (z-step = 2 µm). The IMARIS 9.5 software package (Oxford
424 Instruments) was used to analyse the data.

425

426 **References**

427 1. Bonnans C, Chou J, Werb Z. Remodelling the extracellular matrix in development and disease.
428 *Nat Rev Mol Cell Biol*. 2014;15(12):786-801. doi:10.1038/nrm3904

429 2. Hussey GS, Dziki JL, Badylak SF. Extracellular matrix-based materials for regenerative medicine.
430 *Nat Rev Mater*. 2018;3(7):159-173. doi:10.1038/s41578-018-0023-x

431 3. Fattahi R, Chamkhorami FM, Taghipour N, Keshel SH. The effect of extracellular matrix
432 remodeling on material-based strategies for bone regeneration: Review article. *Tissue Cell*.
433 2022;76(January):101748. doi:10.1016/j.tice.2022.101748

434 4. Mouw JK, Ou G, Weaver VM. Extracellular matrix assembly: A multiscale deconstruction. *Nat Rev*
435 *Mol Cell Biol*. 2014;15(12):771-785. doi:10.1038/nrm3902

436 5. Assunção M, Dehghan-Baniani D, Yiu CHK, Später T, Beyer S, Blocki A. Cell-Derived Extracellular
437 Matrix for Tissue Engineering and Regenerative Medicine. *Front Bioeng Biotechnol*.

438 2020;8(December):1-10. doi:10.3389/fbioe.2020.602009

439 6. Hinderer S, Layland SL, Schenke-Layland K. ECM and ECM-like materials - Biomaterials for
440 applications in regenerative medicine and cancer therapy. *Adv Drug Deliv Rev*. 2016;97:260-269.
441 doi:10.1016/j.addr.2015.11.019

442 7. Tang G, Liu Z, Liu Y, et al. Recent Trends in the Development of Bone Regenerative Biomaterials.
443 *Front Cell Dev Biol*. 2021;9(May):1-18. doi:10.3389/fcell.2021.665813

444 8. Gao C, Peng S, Feng P, Shuai C. Bone biomaterials and interactions with stem cells. *Bone Res*.
445 2017;5(May):1-33. doi:10.1038/boneres.2017.59

446 9. Filippi M, Born G, Chaaban M, Scherberich A. Natural Polymeric Scaffolds in Bone Regeneration.
447 *Front Bioeng Biotechnol*. 2020;8(May). doi:10.3389/fbioe.2020.00474

448 10. Reddy MSB, Ponnamma D, Choudhary R, Sadasivuni KK. A comparative review of natural and
449 synthetic biopolymer composite scaffolds. *Polymers (Basel)*. 2021;13(7).
450 doi:10.3390/polym13071105

451 11. Decaris ML, Leach JK. Design of experiments approach to engineer cell-secreted matrices for
452 directing osteogenic differentiation. *Ann Biomed Eng*. 2011;39(4):1174-1185.
453 doi:10.1007/s10439-010-0217-x

454 12. Harvestine JN, Orbay H, Chen JY, Sahar DE, Leach JK. Cell-secreted extracellular matrix,
455 independent of cell source, promotes the osteogenic differentiation of human stromal vascular
456 fraction. *J Mater Chem B*. 2018;6(24):4104-4115. doi:10.1039/c7tb02787g

457 13. Hoch AI, Mittal V, Mitra D, Vollmer N, Zikry CA, Leach JK. Cell-secreted matrices perpetuate the
458 bone-forming phenotype of differentiated mesenchymal stem cells. *Biomaterials*. 2016;74:178-
459 187. doi:10.1016/j.biomaterials.2015.10.003

460 14. Haumer A, Bourgine PE, Occhetta P, Born G, Tasso R, Martin I. Delivery of cellular factors to
461 regulate bone healing. *Adv Drug Deliv Rev*. 2018;129:285-294. doi:10.1016/j.addr.2018.01.010

462 15. Sadr N, Pippenger BE, Scherberich A, et al. Enhancing the biological performance of synthetic
463 polymeric materials by decoration with engineered, decellularized extracellular matrix.
464 *Biomaterials*. 2012;33(20):5085-5093. doi:10.1016/j.biomaterials.2012.03.082

465 16. Prewitz MC, Seib FP, von Bonin M, et al. Tightly anchored tissue-mimetic matrices as instructive
466 stem cell microenvironments. *Nat Methods*. 2013;10(8):788-794. doi:10.1038/nmeth.2523

467 17. Bourgine PE, Gaudiello E, Pippenger B, et al. Engineered Extracellular Matrices as Biomaterials of
468 Tunable Composition and Function. *Adv Funct Mater*. 2017. doi:10.1002/adfm.201605486

469 18. Pigeot S, Klein T, Gullotta F, et al. Manufacturing of Human Tissues as off-the-Shelf Grafts
470 Programmed to Induce Regeneration. *Adv Mater*. 2021;33(43). doi:10.1002/adma.202103737

471 19. Grigoryan A, Zacharaki D, Balhuizen A, et al. Engineering human mini-bones for the standardized
472 modeling of healthy hematopoiesis, leukemia, and solid tumor metastasis. *Sci Transl Med*.
473 2022;14(666):1-16. doi:10.1126/scitranslmed.abm6391

474 20. Golchin A, Shams F, Karami F. Advancing Mesenchymal Stem Cell Therapy with CRISPR/Cas9 for
475 Clinical Trial Studies. In: *Cell Biology and Translational Medicine,*. Vol 8. ; 2019:89-100.
476 doi:10.1007/5584_2019_459

477 21. Hazrati A, Malekpour K, Soudi S, Hashemi SM. CRISPR/Cas9-engineered mesenchymal
478 stromal/stem cells and their extracellular vesicles: A new approach to overcoming cell therapy
479 limitations. *Biomed Pharmacother*. 2022;156:113943. doi:10.1016/j.biopha.2022.113943

480 22. Geurts MH, Clevers H. CRISPR engineering in adult stem cell-derived organoids for gene repair
481 and disease modelling. 2023;1(January):32-45. doi:10.1038/s44222-022-00013-5

482 23. Hu K, Olsen BR. The roles of vascular endothelial growth factor in bone repair and regeneration.
483 *Bone*. 2016;91:30-38. doi:10.1016/j.bone.2016.06.013

484 24. Duda GN, Geissler S, Checa S, Tsitsilonis S, Petersen A, Schmidt-Bleek K. The decisive early phase
485 of bone regeneration. *Nat Rev Rheumatol*. 2023;19(February):78-95. doi:10.1038/s41584-022-
486 00887-0

487 25. Ran FA, Hsu PD, Wright J, Agarwala V, Scott DA, Zhang F. Genome engineering using the CRISPR-
488 Cas9 system. *Nat Protoc*. 2013;8(11):2281-2308. doi:10.1038/nprot.2013.143

489 26. Otto F, Thornell AP, Crompton T, et al. Cbfa1, a candidate gene for cleidocranial dysplasia
490 syndrome, is essential for osteoblast differentiation and bone development. *Cell*. 1997;89(5):765-
491 771. doi:10.1016/S0092-8674(00)80259-7

492 27. Komori T, Yagi * H., Nomura S, Yamaguchi A. Targeted disruption of. *Proc Natl Acad Sci U S A*.
493 1998;95(15):8692-8697.
494 http://www.pubmedcentral.nih.gov/articlerender.fcgi?artid=21138&tool=pmcentrez&rendertyp
495 e=abstract.

496 28. Kim HJ, Kim WJ, Ryoo HM. Post-Translational Regulations of Transcriptional Activity of RUNX2.
497 *Mol Cells*. 2020;43(2):160-167. doi:10.14348/molcells.2019.0247

498 29. Hattori EY, Masuda T, Mineharu Y, et al. A RUNX-targeted gene switch-off approach modulates
499 the BIRC5/PIF1-p21 pathway and reduces glioblastoma growth in mice. *Commun Biol*.
500 2022;5(1):1-11. doi:10.1038/s42003-022-03917-5

501 30. Kusumbe AP, Ramasamy SK, Adams RH. Coupling of angiogenesis and osteogenesis by a specific
502 vessel subtype in bone. *Nature*. 2014;507(7492):323-328. doi:10.1038/nature13145

503 31. Tuckermann J, Adams RH. The endothelium–bone axis in development, homeostasis and bone
504 and joint disease. *Nat Rev Rheumatol*. 2021;17(10):608-620. doi:10.1038/s41584-021-00682-3

505 32. Largo RD, Burger MG, Harschnitz O, et al. VEGF Over-Expression by Engineered BMSC Accelerates
506 Functional Perfusion, Improving Tissue Density and In-Growth in Clinical-Size Osteogenic Grafts.
507 *Front Bioeng Biotechnol*. 2020;8(July):1-13. doi:10.3389/fbioe.2020.00755

508 33. Yang YQ, Tan YY, Wong R, Wenden A, Zhang LK, Rabie ABM. The role of vascular endothelial
509 growth factor in ossification. *Int J Oral Sci*. 2012;4(2):64-68. doi:10.1038/ijos.2012.33

510 34. Burger MG, Grosso A, Briquez PS, et al. Robust coupling of angiogenesis and osteogenesis by
511 VEGF-decorated matrices for bone regeneration. *Acta Biomater*. 2022;149:111-125.
512 doi:10.1016/j.actbio.2022.07.014

513 35. Behr B, Tang C, Germann G, Longaker MT, Quarto N. Locally applied vascular endothelial growth
514 factor A increases the osteogenic healing capacity of human adipose-derived stem cells by
515 promoting osteogenic and endothelial differentiation. *Stem Cells*. 2011;29(2):286-296.

516 doi:10.1002/stem.581

517 36. Zuo WH, Zeng P, Chen X, Lu YJ, Li A, Wu J Bin. Promotive effects of bone morphogenetic protein 2
518 on angiogenesis in hepatocarcinoma via multiple signal pathways. *Sci Rep*. 2016;6(July):1-9.
519 doi:10.1038/srep37499

520 37. Lowery JW, de Caestecker MP. BMP signaling in vascular development and disease. *Cytokine*
521 *Growth Factor Rev*. 2010;21(4):287-298. doi:10.1016/j.cytogfr.2010.06.001

522 38. Kamekura S, Kawasaki Y, Hoshi K, et al. Contribution of runt-related transcription factor 2 to the
523 pathogenesis of osteoarthritis in mice after induction of knee joint instability. *Arthritis Rheum*.
524 2006;54(8):2462-2470. doi:10.1002/art.22041

525 39. Park DY, Min BH, Park SR, et al. Engineered cartilage utilizing fetal cartilage-derived progenitor
526 cells for cartilage repair. *Sci Rep*. 2020;10(1):1-13. doi:10.1038/s41598-020-62580-0

527 40. Zeng J, Huang L, Xiong H, et al. Injectable decellularized cartilage matrix hydrogel encapsulating
528 urine-derived stem cells for immunomodulatory and cartilage defect regeneration. *npj Regen*
529 *Med*. 2022;7(1):1-12. doi:10.1038/s41536-022-00269-w

530 41. Sekiya I, Vuoristo JT, Larson BL, Prockop DJ. In vitro cartilage formation by human adult stem cells
531 from bone marrow stroma defines the sequence of cellular and molecular events during
532 chondrogenesis. *Proc Natl Acad Sci U S A*. 2002;99(7):4397-4402. doi:10.1073/pnas.052716199

533 42. Pelttari K, Winter A, Steck E, et al. Premature induction of hypertrophy during in vitro
534 chondrogenesis of human mesenchymal stem cells correlates with calcification and vascular
535 invasion after ectopic transplantation in SCID mice. *Arthritis Rheum*. 2006;54(10):3254-3266.
536 doi:10.1002/art.22136

537 43. Mueller MB, Tuan RS. Functional characterization of hypertrophy in chondrogenesis of human
538 mesenchymal stem cells. *Arthritis Rheum*. 2008;58(5):1377-1388. doi:10.1002/art.23370

539 44. Chen Z, Klein T, Murray RZ, et al. Osteoimmunomodulation for the development of advanced
540 bone biomaterials. *Mater Today*. 2016;19(6):304-321. doi:10.1016/j.mattod.2015.11.004

541 45. Xie Y, Hu C, Feng Y, et al. Osteoimmunomodulatory effects of biomaterial modification strategies
542 on macrophage polarization and bone regeneration. *Regen Biomater*. 2020;7(3):233-245.
543 doi:10.1093/rb/rbaa006

544 46. Aamodt JM, Grainger DW. Extracellular matrix-based biomaterial scaffolds and the host
545 response. *Biomaterials*. 2016;86:68-82. doi:10.1016/j.biomaterials.2016.02.003

546 47. Ramakrishnaiah Siddappa, Ruud Licht, Clemens van Blitterswijk J de B. Donor variation and loss of
547 multipotency during in vitro expansion of human mesenchymal stem cells for bone tissue
548 engineering. *J Orthop Res*. 2007;25(8). https://onlinelibrary.wiley.com/doi/10.1002/jor.20402.

549 48. LaFleur MW, Nguyen TH, Coxe MA, et al. A CRISPR-Cas9 delivery system for in vivo screening of
550 genes in the immune system. *Nat Commun*. 2019;10(1):1-10. doi:10.1038/s41467-019-09656-2

551 49. Bock C, Datlinger P, Chardon F, et al. High-content CRISPR screening. *Nat Rev Methods Prim*.
552 2022;2(1). doi:10.1038/s43586-021-00093-4

553 50. Zaqout S, Becker LL, Kaindl AM. Immunofluorescence Staining of Paraffin Sections Step by Step.
554 *Front Neuroanat*. 2020;14(November):1-11. doi:10.3389/fnana.2020.582218

555

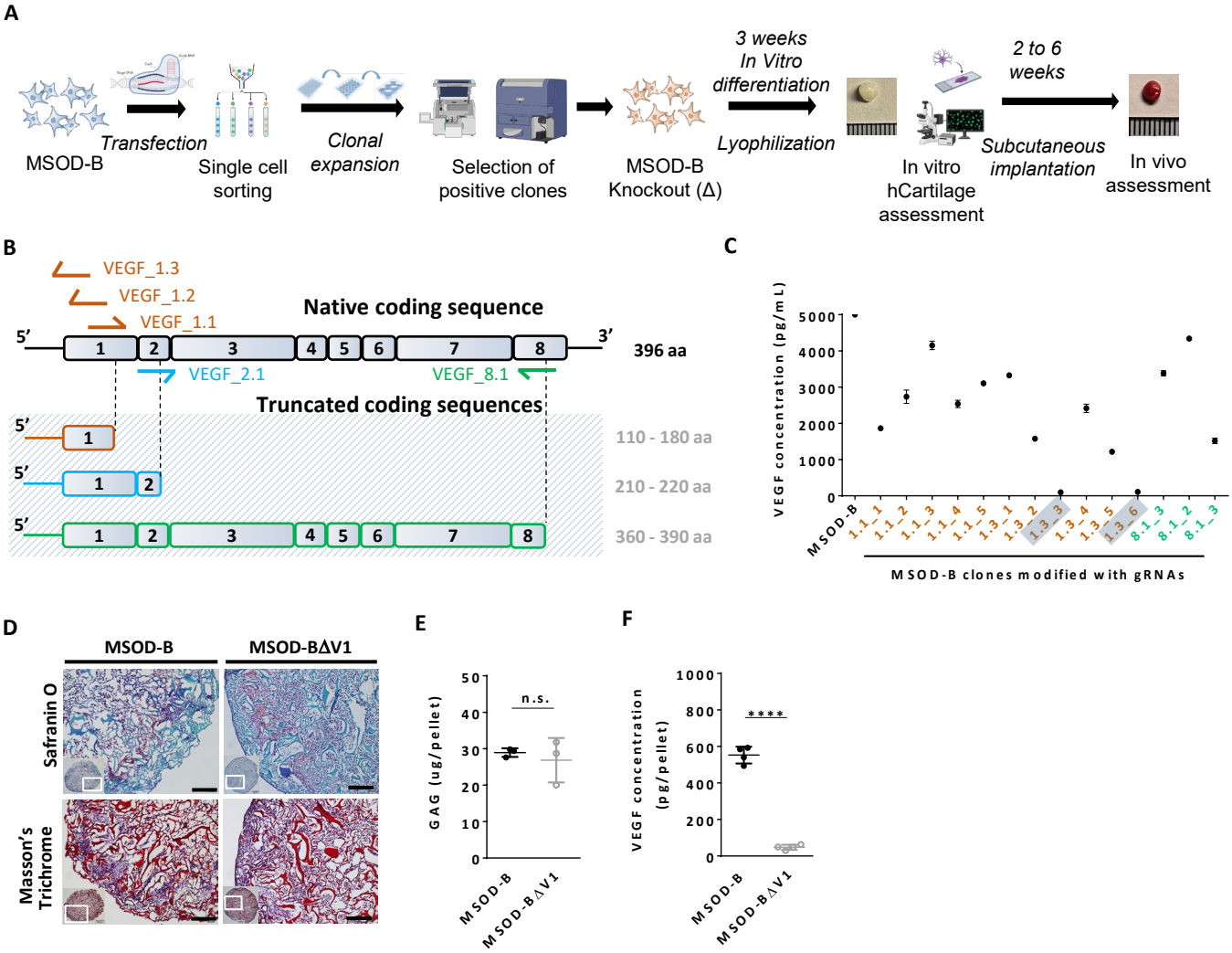

Figure 1. CRISPR/Cas9 editing of mesenchymal cell lines lead to efficient VEGF knockout in cartilage tissues. A) Experimental scheme depicting the generation of CRISP/Cas9-edited MSOD-B lines, and the subsequent in vitro and in vivo tissue formation assessment. B) Overview of the native human VEGF coding sequence composed of eight exons. Designed gRNAs and their targeted binding sites are illustrated, as well as the corresponding expected impact on the coding sequence. gRNAs targeting exon 1 (orange) disrupt translation initiation and inhibit protein expression, gRNA targeting exon 2 (blue) disrupts VEGF receptor binding, and gRNA targeting exon 8 (green) alters the C-Terminal sequence and repress activation of protein. C) ELISA-based quantitative analysis of VEGF protein content in cell culture supernatant from expanded single cell colonies. From all clones, only two had no detectable level of VEGF (1.3_3 and 1.3_6). These clones were subsequently defined as MSOD-BΔV1 and MSOD-BΔV2. D) Histological assessment of in vitro differentiated constructs using Safranin O (top panel) and Masson's trichrome (bottom panel) stains. Both the MSOD-B and MSOD-BΔV1 displayed glycosaminoglycans (GAG) (orange to reddish in Safranin O) and collagen content (Blueish in Masson's trichrome), indicating successful cartilage formation (Scale bars = 200 µm). Left bottom inserts show the whole tissue section. E) Quantitative assessment of the total GAG content in MSOD-B and MSOD-BΔV1 in vitro differentiated constructs. F) ELISA-based quantitative assessment of VEGF protein in in vitro differentiated constructs. Unpaired t-test, n = 3-4 biological replicates, ****$p < 0.0001$, n.s. = not significant.

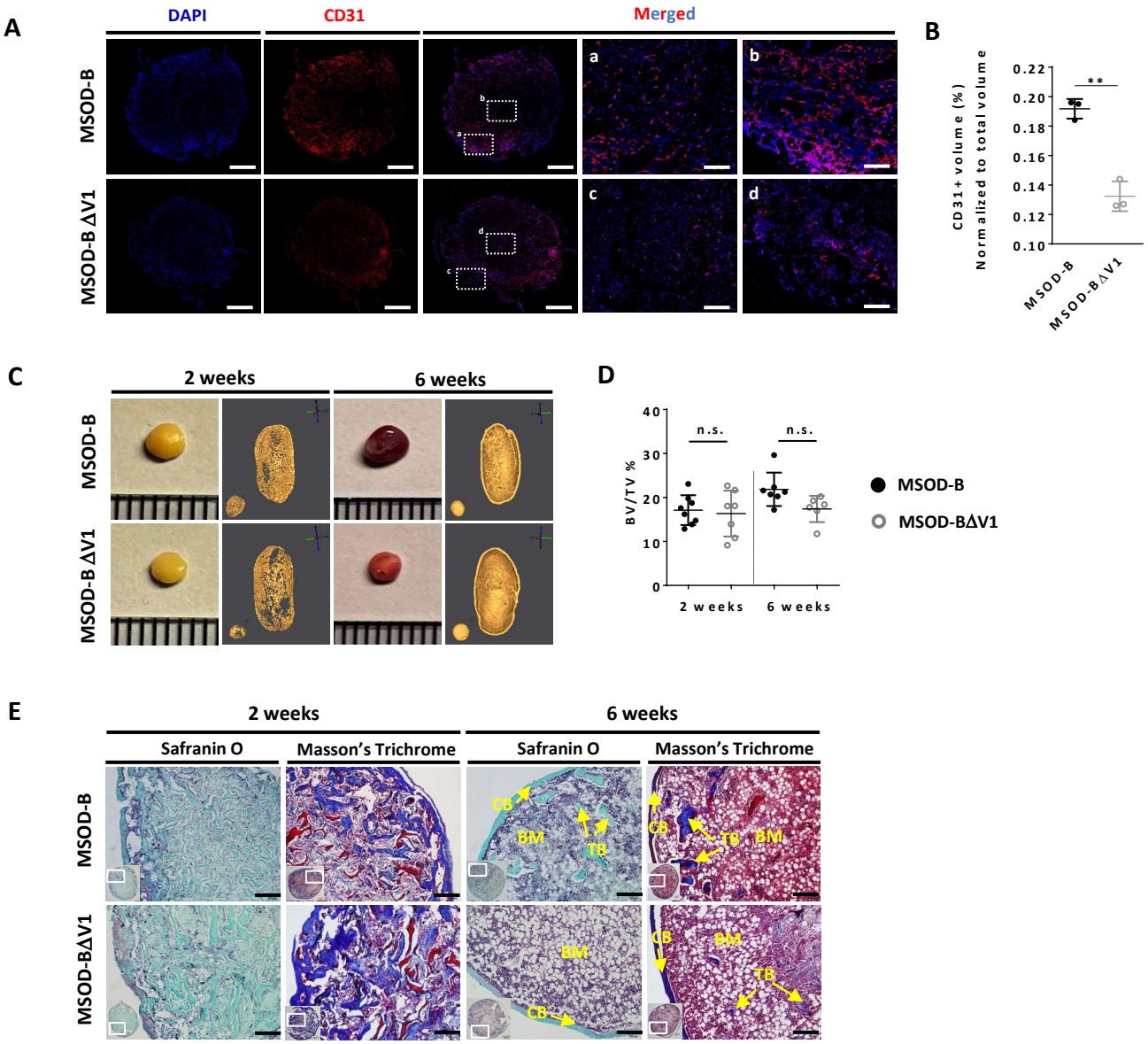

Figure 2. VEGF knockout cartilage tissues retain bone remodeling capacity despite reduced early-stage vascularization A) Immunofluorescence images of MSOD-B and MSOD-BΔV1 tissues two weeks post-in vivo implantation. Displayed images consist of 3D-stacks from 80-100 µm thick sections, vessels stained with mouse CD31 (red) and nuclei with DAPI (blue) (Scale bars at 200 µm except for magnified white inserts at 5µm). Box "a" and "c" display the periphery whereas Box "b" and "d" show the central region of MSOD-B and MSOD-BΔV1 constructs respectively. A reduction in tissue vascularization is observed in MSOD-BΔV1 samples. B) Quantitative analysis of the CD31 signal using an isosurface-based strategy (IMARIS software). C) Representative macroscopic and microtomography images of in vivo constructs retrieved at two and six weeks post-implantation. D) Microtomography-based quantification of the sample's bone/ mineralized volume over their total volume (ratio). No significant differences between MSOD-B and MSOD-BΔV1 could be observed. (BV: Bone Volume, TV: Total Volume). E) Histological analysis of in vivo tissues using Safranin O and Masson's trichrome stains, at two (2W) and six weeks (6W) post-implantation. Both sample types underwent full remodeling into a bone organ after 6 weeks, with presence of bone structures and a bone marrow compartment (Scale bars = 200 µm). CB – cortical bone; BM – bone marrow. TB – trabecular bone. Unpaired t-test, n=3-8 biological replicates, **$p < 0.01$, n.s.=not significant.

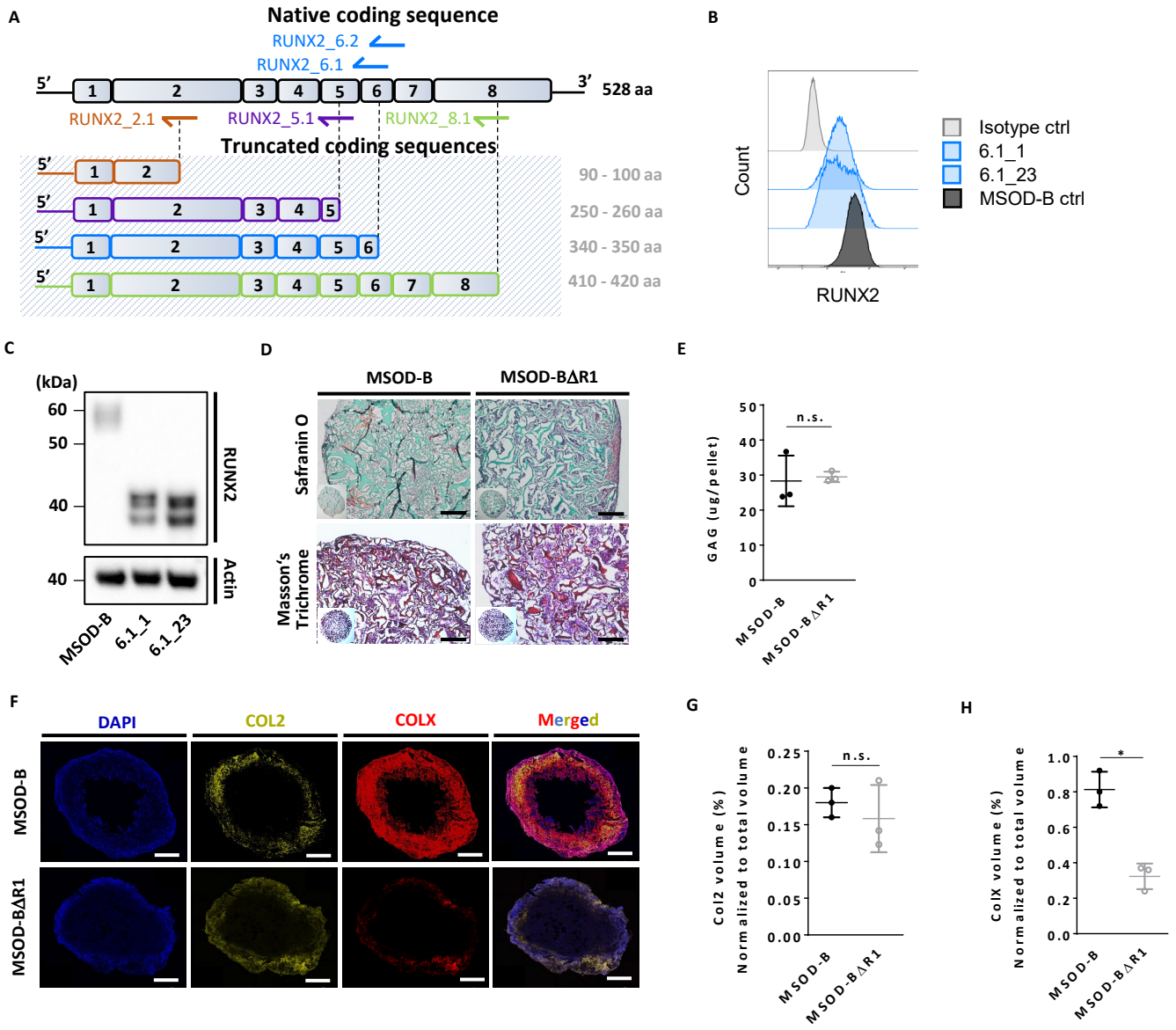

Figure 3. RUNX2 knockout does not prevent chondrogenic differentiation but impairs hypertrophy A) Overview of the human RUNX2 coding sequence comprising 8 exons. gRNAs and their corresponding expected protein structure. The gRNA targeting exon 2 (orange) disrupts the DNA binding domain, gRNA targeting exon 5 (violet) disrupts nuclear translocation, gRNAs targeting exon 6 (blue) disrupt the transcriptional activation domain and gRNAs targeting exon 8 (green) disrupt the nuclear matrix targeting signal and repress the protein function. B) Intracellular flow cytometry for RUNX2 detection in MSOD-B and RUNX2-edited clones. A clear protein reduction could be observed in the 6.1_1 and 6.1_23 clones. C) Western blot analysis of RUNX2 in cultured MSOD-B and RUNX2-edited cells. The genetic editing of RUNX2 is confirmed by the detection of the truncated proteins. Actin is used as a control to normalize the protein content. D) Histological analysis of in vitro constructs using Safranin O (top) and Masson's trichrome (bottom) stains, indicating the presence of cartilage matrices (Scale bars = 200 µm). E) Quantitative assessment of the total GAG content in corresponding in vitro generated tissues. F) Immunofluorescence images of MSOD-B and MSOD-BΔR1 tissues. Displayed images consist of 3D-stacks from 80-100 µm thick sections, stained for DAPI (blue), Collagen Type II (COL2, yellow) and Collagen Type X (COLX, red). A clear reduction in the COLX signal could be observed in the MSOD-BΔR1 tissues, indicating impaired hypertrophy. G) Isosurface-based quantification of the COL2 immunofluorescent signal using the IMARIS software. No significant difference between groups confirm the retention of cartilage formation in RUNX2-edited constructs. H) Isosurface-based quantification of the COLX immunofluorescent signal using the IMARIS software, confirming the disruption of hypertrophy in the MSOD-BΔR1 constructs. Unpaired t-test, n=3, *$p < 0.05$, n.s. = not significant.

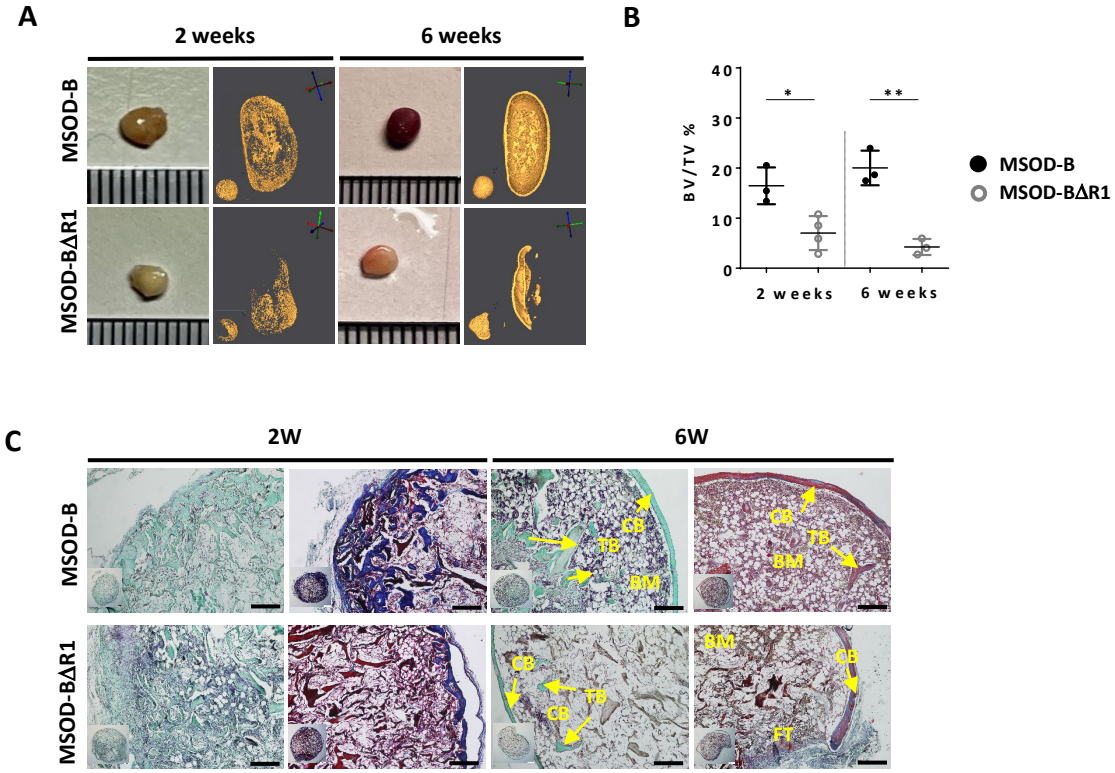

Figure 4. RUNX2 knockout in cartilage tissues disrupts effective bone formation A) Representative macroscopic and microtomography images of in vivo constructs retrieved at two and six weeks post-implantation. B) Microtomography-based quantification of the sample's bone/mineralized volume over their total volume (ratio). (BV: Bone Volume, TV: Total Volume). A marked difference is observed as early as two weeks, with a clear lower mineral content in MSOD-BΔR1 samples. Unpaired t-test, n=3 biological replicates, *$p < 0.05$, **$p < 0.01$. C) Histological analysis of in vivo constructs using Safranin O and Masson's trichrome stains. After two weeks (2W), a higher bone formation is already evident in the MSOD-B control group. The MSOD-BΔR1 samples explanted after 6 weeks (6W) displayed presence of cortical and trabecular bone, but also large amount of fibrous tissue indicating an incomplete remodeling. (Scale bars = 200 µm).